JPL Publication 91-34

Inelastic and Reactive Scattering of Hyperthermal Atomic Oxygen From Amorphous Carbon

Timothy K. Minton
Christine M. Nelson
David E. Brinza
Ranty H. Liang

August 15, 1991

NASA
National Aeronautics and
Space Administration

Jet Propulsion Laboratory
California Institute of Technology
Pasadena, California

JPL Publication 91-34

Inelastic and Reactive Scattering of Hyperthermal Atomic Oxygen From Amorphous Carbon

Timothy K. Minton
Christine M. Nelson
David E. Brinza
Ranty H. Liang

August 15, 1991

National Aeronautics and
Space Administration

Jet Propulsion Laboratory
California Institute of Technology
Pasadena, California

The research described in this publication was carried out by the Jet Propulsion Laboratory, California Institute of Technology, under contract with the National Aeronautics and Space Administration (NASA). The sponsoring NASA agency was the Materials and Structure Division, Office of Aeronautics and Exploration Technologies.

ABSTRACT

The reaction of hyperthermal oxygen atoms with an amorphous carbon-13 surface has been studied using a modified universal crossed molecular beams apparatus. Time-of-flight distributions of inelastically scattered O-atoms and reactively scattered ^{13}CO and $^{13}CO_2$ were measured with a rotatable mass spectrometer detector. Two inelastic-scattering channels were observed, corresponding to a direct inelastic process in which the scattered O-atoms retain 20-30 percent of their initial kinetic energy and to a trapping desorption process whereby O-atoms emerge from the surface at thermal velocities. Reactive-scattering data imply the formation of two kinds of CO products, 1) slow products whose translational energies are determined by the surface temperature and 2) hyperthermal ($\sim$3 eV) products with translational energies comprising roughly 30 percent of the total available energy (E_{avl}), where E_{avl} is the sum of the collision energy and the reaction exothermicity. Angular data show that the hyperthermal CO is scattered preferentially in the specular direction. CO_2 product was also observed, but at much lower intensities than CO and with only thermal velocities.

Contents

I. INTRODUCTION

Atomic oxygen in low Earth orbit (LEO, 200-700 km), combined with high orbital velocities, gives rise to hyperthermal oxygen atom reactions on satellite surfaces. The typical O-atom number density at space shuttle altitudes is on the order of 10^8 cm^{-3}. An orbiting body traveling at 8 km/sec through this density experiences a flux of $\sim 10^{14}$ O-atoms/cm^2/s. The high velocity atomic oxygen impacts correspond to collision energies of 5 eV (480 kJ/mol), and the $\sim$1000 K ambient temperature gives an energy spread of 3.9-7.0 eV to the collisions. The atomic oxygen concentration is dependent on many factors besides altitude, including solar activity, season, and variations in the Earth's magnetic field, latitude, and local time.[1, 2] Model calculations (e.g., MSIS-86[2, 3]) are usually used to calculate atomic oxygen number densities encountered for a particular mission.

The detrimental effect of hyperthermal oxygen atom reactions on material surfaces was first recognized after post-flight analyses of polymer and paint surfaces which were exposed during early space shuttle flights (STS-1, STS-2, STS-3).[4] Polymers showed a loss of surface gloss and concomitant weight loss, while paint surfaces exhibited premature aging. Initial concern over the degradation of materials by atomic oxygen sparked a huge effort aimed at the identification, understanding, and solution of problems caused by O-atoms in LEO.[5, 6] These problems can be classified and summarized as follows:

- **Erosion** of materials (optical and thermal control coatings, carbon-based composites, thermal blankets, solar panels, optical components). Fast O-atoms react directly with a surface, and volatile reaction products are ejected. The reaction products can subsequently be a source of contamination. The remaining material will not only be structurally weakened, but the altered surface morphology

will reduce specular reflectance. Erosion of a graphite-epoxy matrix can release carbon fibers, which are a hazard to electronics. Finally, atomic oxygen can act in combination with ultraviolet (UV) and vacuum ultraviolet (VUV) radiation to erode materials (e.g., FEP Teflon[7]) which are not eroded by either atomic oxygen or UV and VUV alone.

- **Oxidation** of materials. While not eroded, materials may still oxidize and take on new thermal and radiative properties. A lubricant, such as molybdenum disulfide (MoS_2), can be oxidized to an abrasive oxide.[8] Oxidation can also cause dimensional changes – e.g., silicone will form a surface oxide layer which can contract and crack; oxidation of silver produces expansion and spalling.

- **Indirect impingement**. Elastically and inelastically scattered oxygen atoms can cause oxidation and, possibly, erosion of materials shadowed from direct attack.

- **Glow**. Surface-assisted reactions between oxygen and nitrogen yield chemiluminescent products, thus creating a glow which could seriously interfere with the function of sensitive optical instruments designed to detect low light levels.

The most basic approach to the materials erosion problem is simply to make the material thicker, so that any mass loss would be insignificant compared to the overall mass loss of the piece. This approach would be limited to applications, such as structures, where a change in surface morphology would not matter. An obvious problem with making thicker, heavier structures is the added energy, and therefore cost, required to deposit them into orbit. The microgravity of the space environment allows the use of very thin structures, whose integrity would be diminished by long term atomic oxygen induced erosion.

Additives or modifications to existing materials can potentially reduce the reaction rate of a material with atomic oxygen. For example, siloxane modified polyimides have an O-atom reactivity of about 10 times less than the commonly used polyimide, Kapton. The siloxane-polyimide block copolymers are effective because they react with atomic oxygen to form a protective layer of silicon dioxide.[9] The ability of the material to form its own protective coating makes it somewhat self-healing if the surface is disrupted by an impact from a micrometeoroid or space debris.

Protective coatings provide another means to combat O-atom degradation of materials. The viability of many coatings has been considered. Some, such as PTFE Teflon, silicon dioxide, aluminum oxide, and silicone, have been tested. While coatings show some promise, many problems must be overcome. Tiny defects in a coating allow oxygen atoms to penetrate to the reactive material underneath the coating, where, over time, extensive undercutting around the defect can occur. Furthermore, some unreactive coatings (e.g., Al_2O_3) allow O-atoms to diffuse through.[10] Even a high quality, atomic oxygen resistant coating is susceptible to damage from micrometeoroids and debris. Current data on coatings are fairly crude because studies are hampered by lack of control of many parameters, including temperature, coating continuity, coating impurities, and substrate surface roughness. Although coatings have their drawbacks, their development will continue because coatings are our most effective means at this time to shield vital spacecraft components from oxygen atom attack.

So far, proposed solutions to the atomic oxygen problem are imperfect. The low Earth orbit environment is extremely harsh, and few non-metallic materials can withstand it, especially for long periods of time. Our ever increasing understanding of the nature of fast O-atom interactions with materials might well lead to the development

of a new generation of atomic oxygen resistant materials that will obviate the need for such band-aid approaches as those mentioned above. At the least, a good foundation of knowledge will be invaluable to the design of systems that will put imperfect materials to their best uses.

In this report, we focus on two of the issues mentioned above – erosion and indirect impingement. The quest for ground-based facilities which accurately simulate degradation resulting from oxygen atom reactions in the LEO environment has led to the development of many O-atom test facilities,[11] in which the erosion rates of various materials can be measured. Naturally, reliable ground-based materials evaluations are sought after as an economical alternative to space experiments. But the data generated so far are unreliable; reproducibility of results at different sites is rare. No testing method has been shown to give an accurate representation of the space environment, and no experiment has even been calibrated with space data. One problem of relating space data to ground-based results is the lack of accurate experiments in space (a void which should be filled with the flight of the EOIM-III experiment in 1992). Still a more profound problem is the inherent difficulty of making neutral, ground state, hyperthermal oxygen atoms in the laboratory. Some deal with this problem by producing low kinetic energy O-atoms; many use plasma ashers, and others create O^+ and O_2^+ ions. With one exception, all sources of 5 eV O-atoms (including ours) have as by-products UV and VUV light, ions, excited state species, and fast neutrals such as O_2 and rare gas atoms. These by-products may affect apparent erosion rates by acting either alone or in combination with O-atoms to degrade a sample. The one "clean" 5 eV O-atom source[12] is not used for conventional erosion studies because of its small beam size and relatively low flux. Given the limitations on producing an ideal oxygen atom beam for ground-based studies, it might never be possible to

obtain accurate erosion data through a precise simulation of LEO.

Perhaps a more prudent approach would be to discover the mechanisms of the interactions of O-atoms with materials. Even without an ideal beam source, controlled experiments can be performed in order to deduce the reaction mechanisms. The mechanisms provide the essential information needed to create models which can be used to predict longevity in LEO. Knowledge of a reaction mechanism can also aid in the interpretation of exposure data so that meaningful conclusions can be drawn. The paucity of data on the detailed interaction between fast oxygen atoms and a reactive surface motivated our study of the reaction of hyperthermal oxygen atoms with a carbon surface. While some work on this relatively simple interaction has been reported,[13–15] even such basic properties as the identity of the scattered products and their translational energies still remain unknown.

Our interest in the O + C reaction is practical as well as fundamental. Graphite and carbon composites are used for structural members on spacecraft. However, the integrity of these structures can be compromised in LEO because carbon is susceptible to erosion by hyperthermal oxygen atoms.[16] Because the O-atom/carbon system involves only two elements, the number of possible scattering processes is limited to three: 1) inelastic (or elastic) scattering of O-atoms, 2) reactive scattering to produce CO, 3) reactive scattering to produce CO_2. The importance of carbon for use in LEO and the limited number and the simplicity of possible scattering products make the O + C interaction a model system for the mechanistic study of hyperthermal O-atom interactions with materials.

II. EXPERIMENT

The apparatus used has been described previously,[17] and it will be briefly reviewed here. The JPL Crossed Molecular Beams Apparatus, or CMBA, (see Fig. 1) is a duplicate of an instrument originally designed by Y. T. Lee and coworkers[18] for the specific purpose of studying fundamental gas phase reaction dynamics. Scattering experiments with crossed molecular beams offer the most direct means to study the dynamics of elementary chemical reactions. These experiments have yielded much detailed information about angular distributions of products; disposal of reaction exothermicity among translation, rotation, and vibration; lifetimes of intermediate collision complexes; variation of reaction cross section with collision energy and impact parameter; and the correlation of reaction dynamics with electronic structure. Such information is accessible with the CMBA in large part as a result of the CMBA's versatile detector design, utilizing a rotatable mass spectrometer.

The detector is a quadrupole mass spectrometer with electron bombardment ionization and is housed in differentially pumped chambers to minimize background. The entire detector unit, including pumps and cryogenic trap, is mounted on a rotatable platform (angular range 170°) which forms the lid of the scattering chamber. The beam sources are modular units, mounted in differentially pumped side chambers which insert into the scattering chamber. Angular distributions of reaction products are obtained by rotating the detector about the collision, or interaction, zone of the two beams, and product velocity distributions are measured by the time-of-flight (TOF) method with the aid of a chopper wheel in front of the detector. Although the apparatus was originally designed for the study of gas phase reactions, its versatile design makes it well suited to the study of heterogeneous gas-surface reactions. The oxygen atom scattering experiments described here were performed by inserting a

JPL Fast Atomic Oxygen Exposure Facility

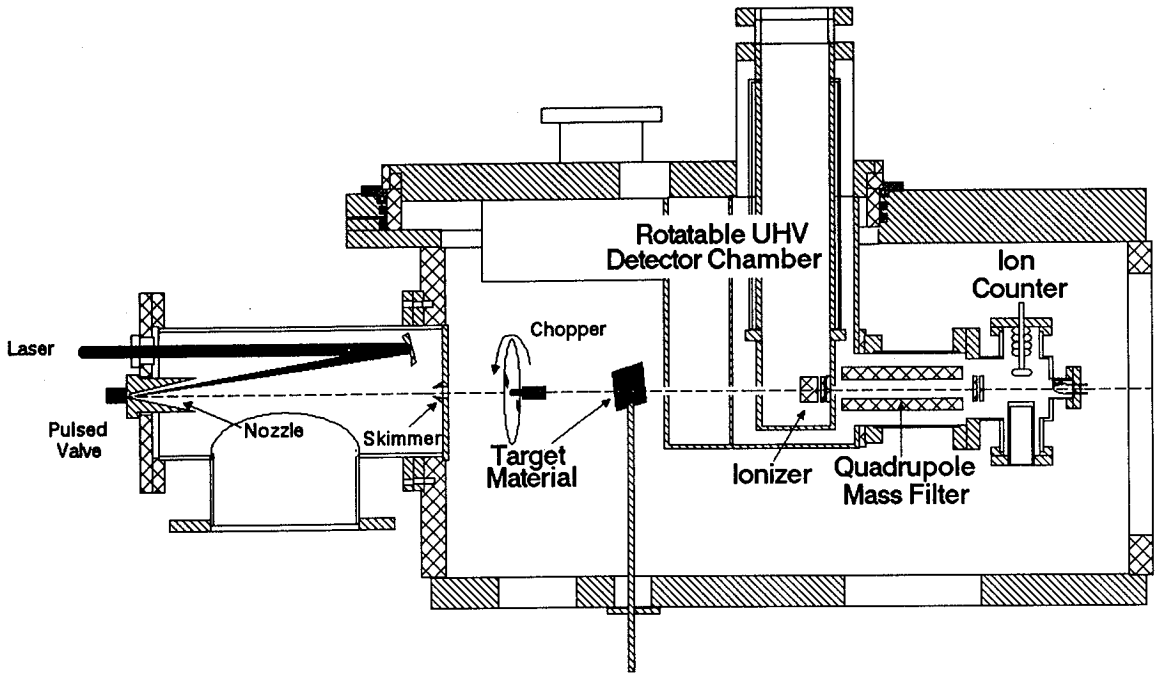

Figure 1. Schematic representation of the crossed molecular beams apparatus configured for the study of hyperthermal oxygen atom reactions with surfaces.

carbon target in the interaction region and directing a pulsed beam of hyperthermal oxygen atoms at the target. The incident beam passed through an aperture, which restricted the beam spot to a 3mm × 3mm square cross section at the interaction region. The angle of incidence between the molecular beam and the target was typically 45°, and with one exception, all scattered species were detected at 90° to the incident beam.

Both scattering and source chambers are pumped by oil diffusion pumps that are water-baffled to reduce backstreaming. Because silicone contamination can lead to a protective SiO_2 layer on the surface,[19] non-silicone diffusion pump fluids were used, i.e., Santovac 5 for the scattering chamber and Fomblin for the source. Typical pressures during an experiment were 2×10^{-7} torr in the scattering chamber and 5×10^{-5} in the source chamber.

The carbon target, supplied by Arizona Carbon Foil, was prepared by sputter coating carbon-13 onto a 1 × 1 inch aluminum substrate. The target was rinsed with clean methanol and CCl_2FCClF_2 before insertion into the scattering chamber. All scattering data for a particular set of O-atom beam conditions were collected without moving the target. The target was moved between experiments to provide a fresh interaction spot for the slightly altered O-atom beam. Beam TOF distributions were averaged for 100-200 laser shots, while reactive-scattering TOF distributions were averaged for as many as 2000 shots.

The oxygen atom beam source is a copy of a source developed by Physical Sciences, Inc.[20] In our source, a pulsed valve (General Valve, Series 9) is used to introduce oxygen gas at a stagnation pressure of 80 psig into an uncooled conical nozzle made of copper. Approximately 450 μs after the valve is triggered, a pulsed CO_2 laser (Altec 851) is fired, and the ~5 joule pulse is focussed into the throat of the nozzle by a

gold mirror with a 50 cm radius of curvature. The intense field induces a breakdown in the nozzle, creating a plasma which strongly absorbs the laser light. The net effect is an instantaneous heating of the O_2 gas to temperatures over 20,000 K, where virtually complete dissociation and partial ionization occur. A large fraction of the laser energy is channeled into translation of the radicals and ions. The shape of the nozzle, coupled with the relatively high density of the plasma, promotes electron-ion recombination and collisional relaxation of the excited species. While the resulting beam from the nozzle consists predominately of fast oxygen atoms, fast molecular oxygen is also generated, presumably by a three-body recombination process or by entrainment of residual O_2. In addition, some ionized and excited state species persist even after the expansion from the nozzle. Finally, unprocessed thermal O_2 is in the beam in varying amounts depending on the exact initial source conditions.

The molecular beam is characterized by measuring the TOF distribution of the pulse with the mass spectrometer detector. The detector is rotated such that the molecular beam and detector axes coincide. (A 0.005 inch diameter orifice is used as an aperture on the front of the detector for beam characterization, while a 3mm $\times$ 3mm square aperture – acceptance angle 3° – was employed for the detection of scattered products.) An EG&G Ortec ACE-MCS multichannel scaler was used to collect ion counts as a function of arrival time in the detector. All data were collected with a dwell time of 10 μs. Figure 2 illustrates a typical beam as measured by the TOF method. The multichannel scaler is triggered at the same time as the pulsed valve. After 450 μs, the CO_2 laser is fired, and a signal spike arising from VUV light produced in the plasma is seen. This spike serves as a convenient time zero marker for the O-atom beam. Figure 2a shows the TOF distribution seen at a mass-to-charge ratio (m/q) of 16. The signal with a peak at 620 μs arises from

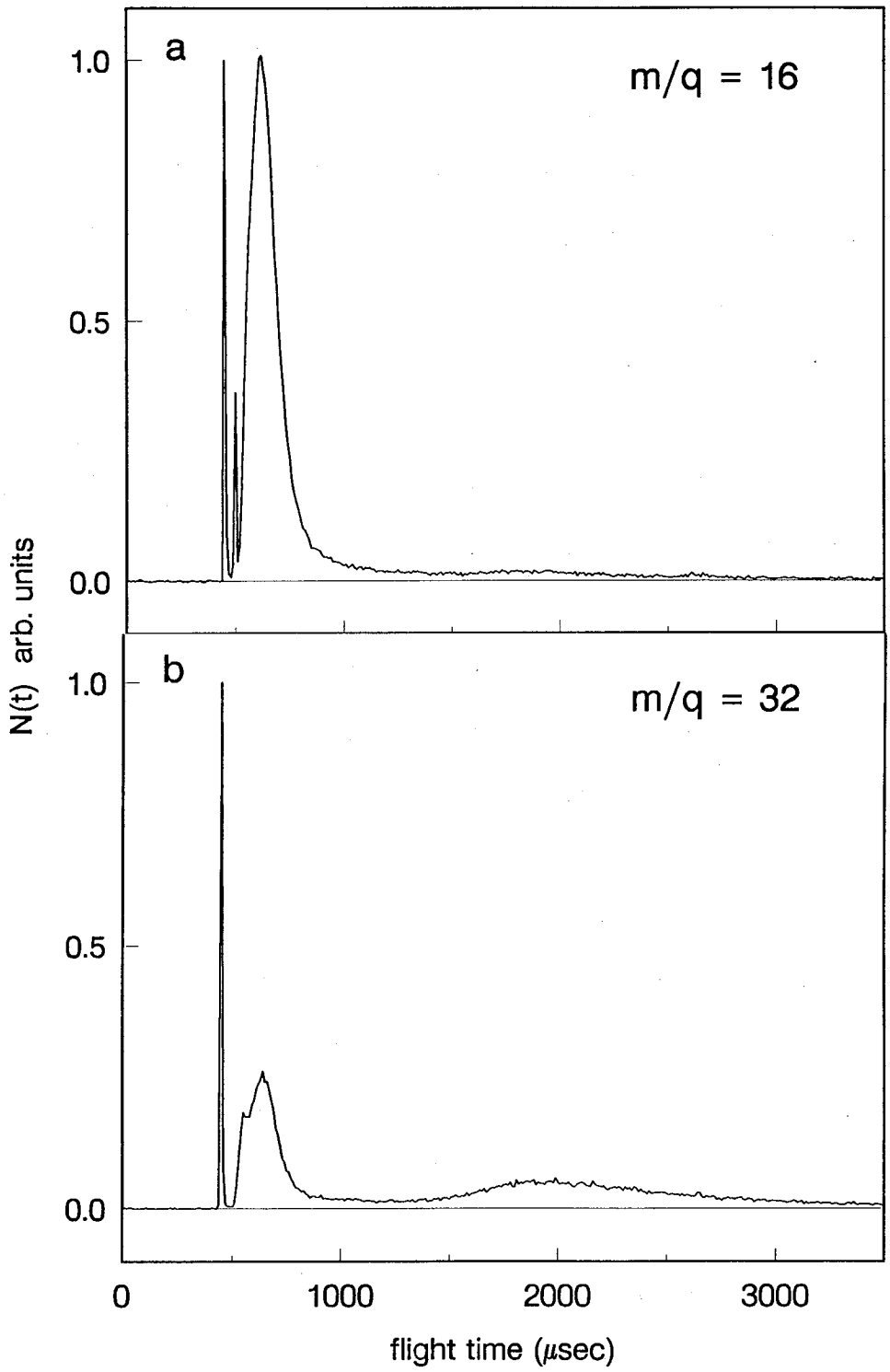

Figure 2. TOF distributions of a representative pulsed oxygen atom beam detected at two different mass-to-charge ratios.

hyperthermal O-atoms, and the small signal at about 2 ms comes from thermal O_2 that is dissociatively ionized to m/q=16 in the ionizer. (The detected signal of O_2 at m/q=16 is about 30 percent of that seen at m/q=32.) Figure 2b shows the same beam detected at m/q=32. As mentioned above, some fast O_2 is produced in the beam, which in this case gives rise to a signal at ~700 μs. Again, residual thermal O_2 gives a signal around 2 ms. In both TOF distributions, a sharp spike is seen at very short times relative to the fast O-atom or O_2 peaks. The origin of this spike is unclear, although observations suggest it could come from Rydberg atoms. It is seen at every mass and even with the ionizer off. An electric field applied to the beam fails to reduce the spike's intensity. Its magnitude does, however, depend strongly on the initial source conditions. The data discussed in this report appear to be insensitive to this spike, so it will be ignored in the analysis.

The raw TOF data, such as that presented in Fig. 2, must be corrected for the transit time of the ionized species from the ionizer through the mass filter to the Daly-type ion counter. This ion flight time is given by $\alpha\sqrt{m/q}$ (for a particular ion energy), where m/q is the mass-to-charge ratio and α is an empirically determined proportionality constant, which for our detector conditions has not yet been determined. For fast signals, the ion flight time becomes critical in the determination of the corresponding translational energy.

Key parameters of our apparatus which enable us to perform a rough analysis of the energetics of O-atom scattering are the distance from the source to the ionizer – 129 cm – and the distance from the interaction region to the ionizer – 34.0 cm.

In this report, the results from four data sets, representing four different O-atom beam conditions, will be discussed. For the purposes of discussion, we will label the beams as follows: BEAM I, BEAM II, BEAM III, and BEAM IV. BEAM III is the

only case where the beam was not at a 45° angle of incidence with respect to the carbon surface; the angle of incidence was instead 51°. The BEAM IV data set was the only one in which a chopper wheel was used between the source and the target (see Fig. 1). The chopper wheel had four tabs on it, and it was spun at 200 Hz. The timing was adjusted such that the fastest part of the beam, as well as the light from the plasma, was blocked. For all data sets, TOF distributions of the beam were collected at m/q=16 and 32 with the target lowered out of the beam path. The target was then raised into the beam so scattering data could be obtained. Depending on the experiment, TOF distributions of scattered species were recorded at m/q=16, 29, 32, or 45.

III. RESULTS AND ANALYSIS

A. Atomic oxygen translational energy distributions

The translational energy distributions $P(E_B)$ of the oxygen atom beams were derived from the measured TOF distributions $N(t_B)$ of the pulsed beams. Corrected $N(t_B)$ distributions for m/q=16 were obtained by subtracting the appropriately scaled m/q=32 signal after adjusting both distributions for an estimated flight time. The resulting m/q=16 TOF distributions are shown in Fig. 3. The fits to the distributions in Fig. 3 were derived by using the relationship $N(t_B) \propto P(E_B)/t^2$. Average translational energies are included with the $P(E_B)$ distributions in Fig. 4. The uncertainty in flight time, resulting from the lack of knowledge of the ion flight time and from the coarse 10 μs increments in which the data were collected, make the derived translational energy distributions in Fig. 4 uncertain by perhaps as much as 30 percent.

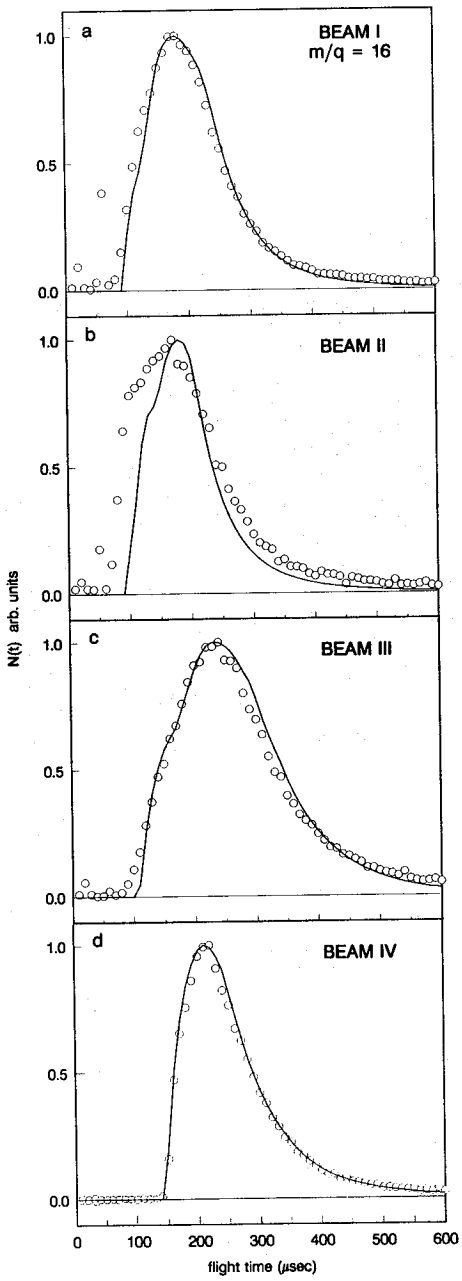

Figure 3. O-atom TOF distributions of four beams used for studies described in this report. The circles are experimental data points, and the solid lines are fits calculated using the translational energy distributions in Fig. 4. The fast signal in (b) was not fitted because it arose from an anomalous fast spike often seen in the beam TOF data.

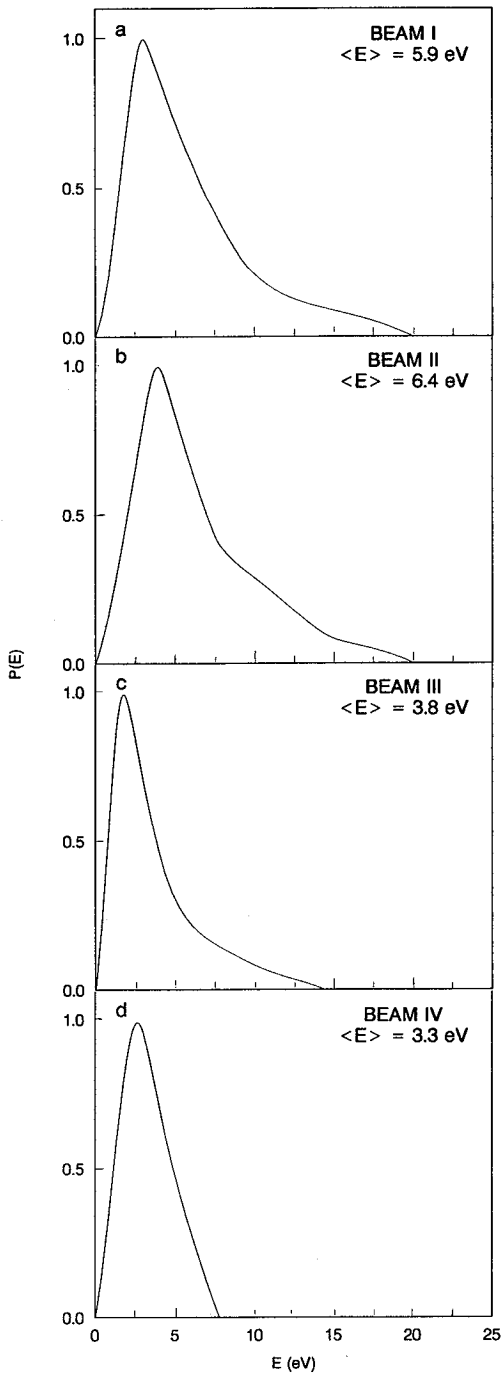

Figure 4. Translational energy distributions used to fit the O-atom beam TOF distributions in Fig. 3. Shown with each $P(E)$ distribution is the corresponding average translational energy of the O-atoms in the pulsed beam.

B. Inelastic scattering

TOF distributions of O-atoms scattered from the carbon target were recorded for BEAM I and BEAM IV conditions (Fig. 5). These distributions are a convolution of the incident beam distribution with the scattered O-atom distribution, thus limiting the information that can be obtained from them. Furthermore, the slow scattered O-atom signal is obscured by inelastically scattered thermal O_2.

We would like to find the translational energy distribution of scattered O-atoms for a given incident energy, but the broad energy range of the current beam makes this goal unobtainable. We have no way of correlating incident energy with scattered energy. Nevertheless, we can derive an approximate average energy for scattered oxygen atoms by assuming that the scattered atoms have no memory of the incident beam. Therefore, the incident beam is assumed to contribute to the scattered O-atom $P(E_S)$ distribution only insofar as it gives rise to a distribution of impingement times at the target surface. This time distribution can easily be determined from the relation $P(t_B) = P(E_B)dE_B/dt_B \propto P(E_B)/t_B^3$. The method by which $P(E_S)$, the translational energy distribution of scattered O-atoms, is derived can be summarized as follows: 1) guess $P(E_S)$; 2) calculate $N(t_S)$ from the $P(E_S)$; 3) weight this $N(t_S)$ by $P(t_B)$; 4) compare this result with the observed TOF distribution; and 5) repeat until a satisfactory match is obtained. This method should in principle be valid when $P(E_B)$ and $P(E_S)$ are completely uncorrelated. In addition, a practical limitation exists when $P(E_B)$ is very broad, as in our experiments, because the width of the observed TOF distribution of scattered O-atoms is determined mainly by the wide time range of oxygen atoms striking the surface. Figure 5a shows an example in which the assumed $P(E_S)$ is very narrow (FWHM 0.052 eV) and the calculated TOF distribution is relatively broad. Because of the possible errors inherent in the analysis

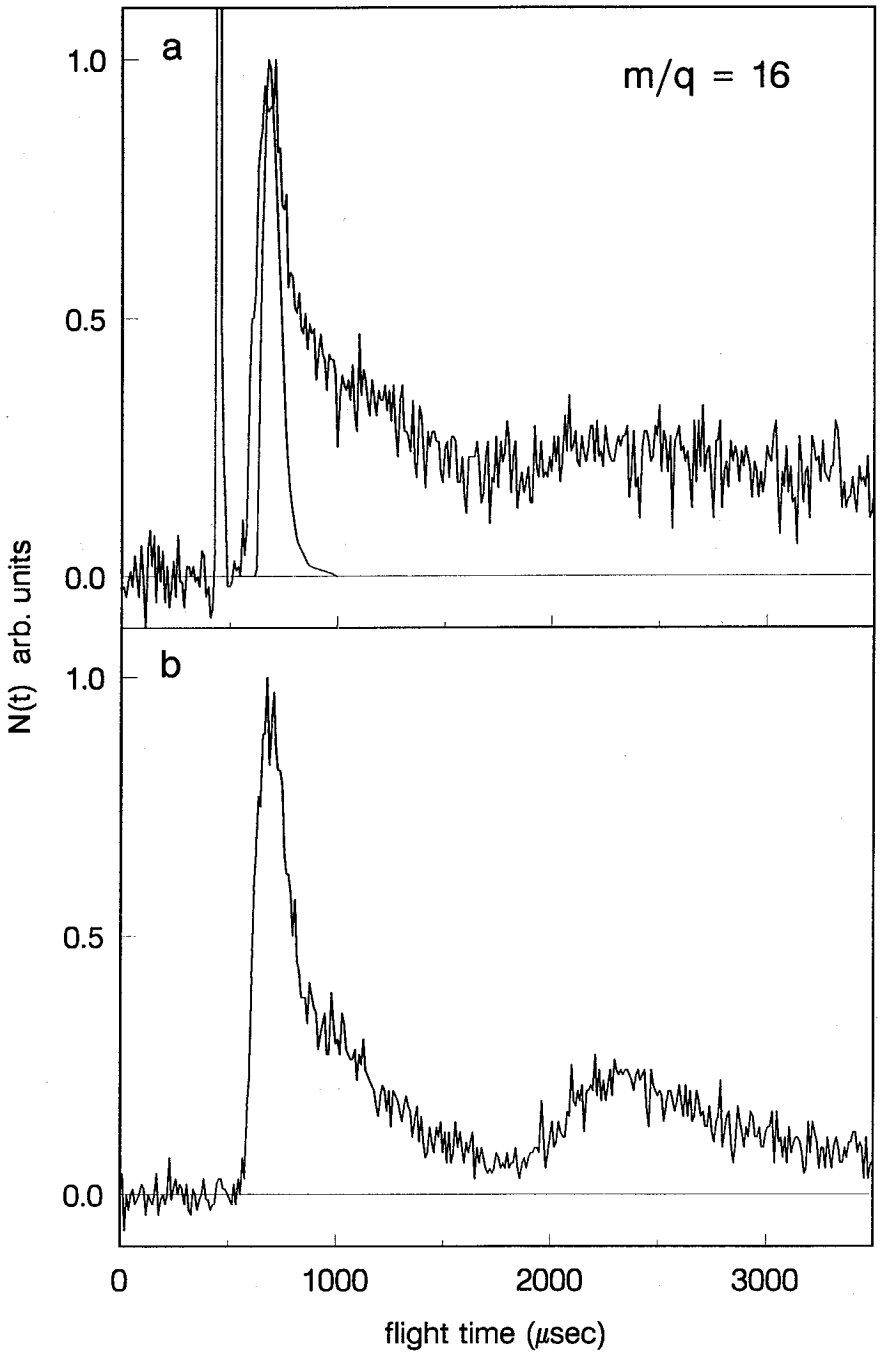

Figure 5. TOF distributions of O-atoms scattered from the carbon target using BEAM I (a) and BEAM IV (b) conditions. Shown in (a) is a TOF distribution that was calculated by assuming a translational energy distribution of scattered O-atoms with a width (FWHM) of 0.052 eV.

and the insensitivity of the data to the shape of the scattered O-atom translational energy distribution, we report only approximate energies of the scattered O-atoms and not an entire $P(E_S)$ distribution.

The inelastic-scattering signal in Fig. 5a shows a sharp fast peak and a slow shoulder. Although these two components appear overlapped in the TOF distribution, they correspond to very different energy O-atoms scattered from the surface. The slow component comes from O-atoms with translational energies of ~0.05 eV (i.e., $2RT$, the thermal energy associated with desorption from a 300 K surface), and the fast component corresponds to O-atoms with translational energies around 1.2 eV. The second experiment in which O-atom inelastic-scattering data were collected showed very similar results (Fig. 5b). In both cases, a fast component, corresponding to a 70-80 percent loss of initial kinetic energy, and a slow component, corresponding to O-atoms with roughly thermal velocities, were present.

C. Reactive scattering

Reactive-scattering data were collected with three beam conditions, BEAM I, BEAM II, and BEAM III. With BEAM I and BEAM II, a single TOF distribution at m/q=29 (CO^+) was collected, and with BEAM III, TOF distributions at m/q=29 were collected at two different detector angles. In addition, a single TOF distribution at m/q=45 (CO_2^+) was recorded with BEAM II.

Figure 6 shows the m/q=29 TOF distribution taken with BEAM I conditions. An immediately striking result is the existence of two peaks. This observation is reproduced with BEAM II as seen in Fig. 7a. However, the m/q=45 TOF distribution (Fig. 7b) exhibits only one relatively slow peak. (It should be noted that the two distributions shown in Fig. 7 were obtained with different detector conditions, which in effect gave an ion collection efficiency for the m/q=45 TOF distribution of approximately

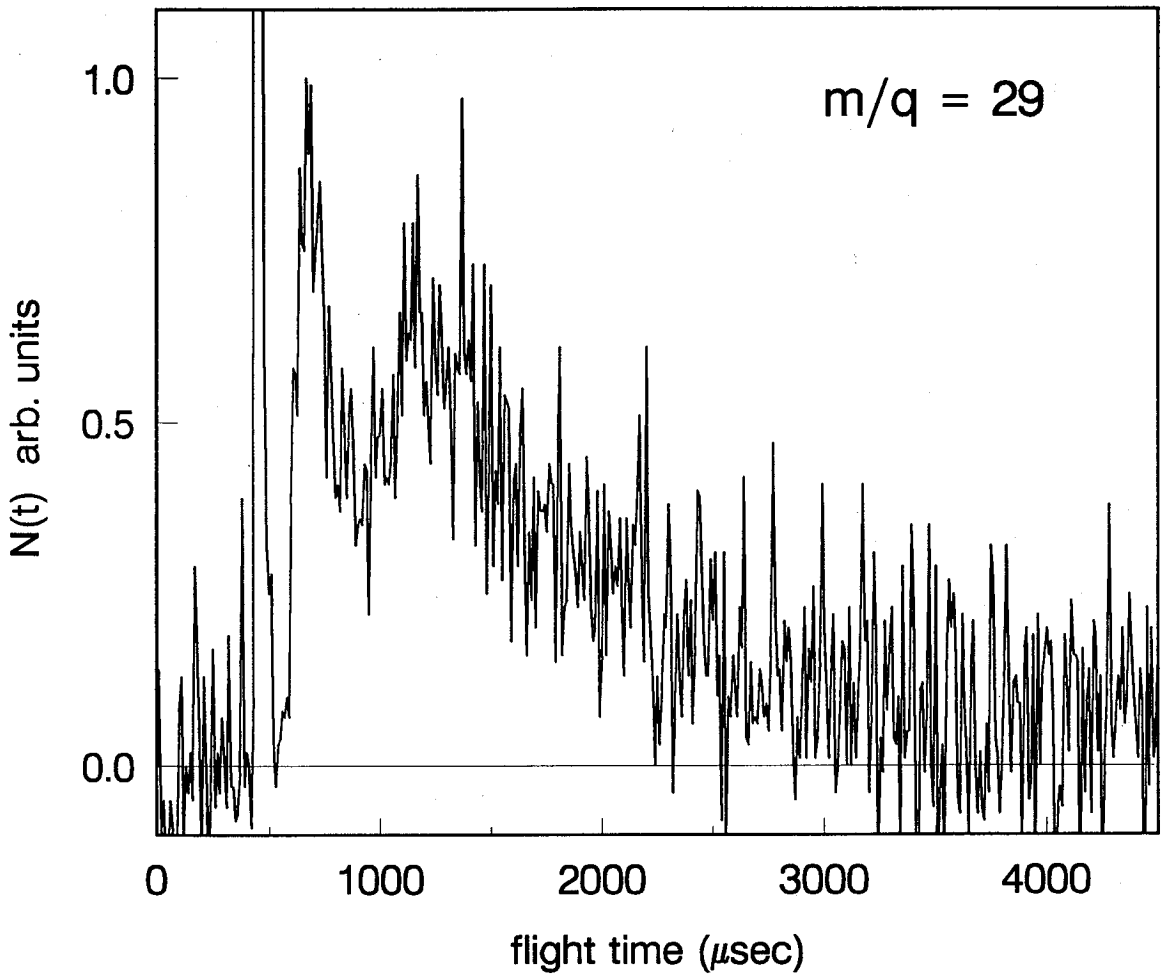

Figure 6. TOF distribution of reactively scattered ^{13}CO using BEAM I conditions.

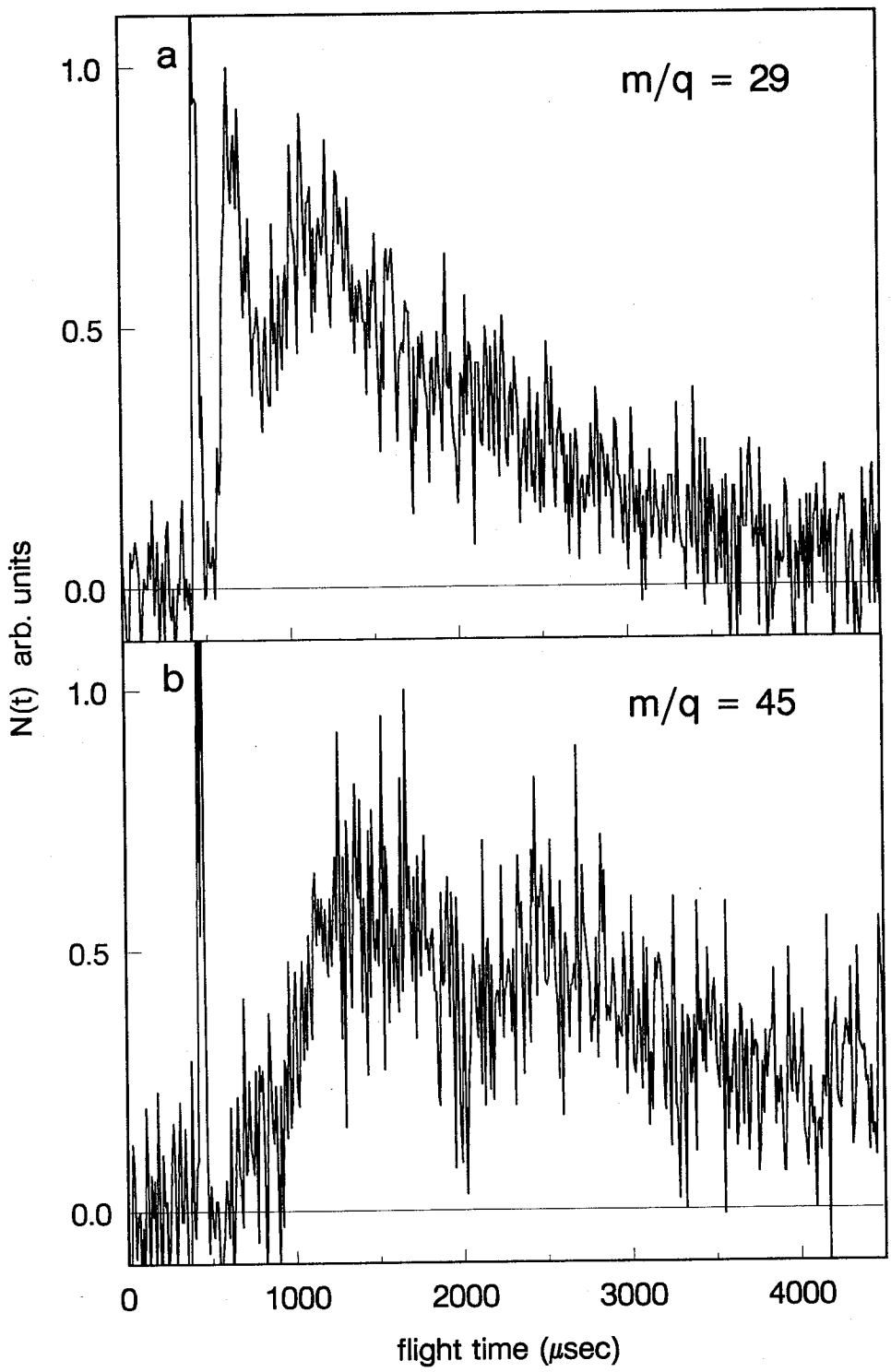

Figure 7. TOF distributions of reactively scattered ^{13}CO (a) and $^{13}CO_2$ (b) using BEAM II conditions.

twice that for the m/q=29 TOF distribution.) All scattering data contain a very slow (~2 ms) signal that is the result of a thermal component of the beam. At m/q=29, a small amount of mass leakage from thermal O_2 can be detected, and at m/q=45, the resolution setting of the mass filter was low enough that an m/q=44 signal was detected, possibly as a result of a low level of CO_2 impurity in the beam. In order to make sure that no CO impurity in the beam was producing a signal at m/q=29, we collected an m/q=28 TOF distribution, which showed essentially no signal.

The BEAM III data provide some information on the angular dependence of the m/q=29 signal. After insertion of the target into the interaction region, the detector was set at the specular angle by rotating it until the light spike was maximized. The resulting detector angle was 102° with respect to the beam. Hence, the angle of incidence was 51°. An m/q=29 TOF distribution was recorded at this angle (Fig. 8a), then the detector was rotated 17° toward the surface normal and another m/q=29 distribution was recorded (Fig. 8b). A third TOF distribution (Fig. 8c) was taken at the original angle as a check to make sure a drift in beam or detector conditions was not causing spurious results. Although a slight drift occurred, the magnitude of the fast peak relative to the slow signal is clearly dependent on the detection angle, with the specular direction yielding the largest fraction of fast CO component.

Based on the analysis outlined in part B, the approximate translational energy for all hyperthermal CO products observed with all three beam conditions is 3 eV. In addition, it is clear that some CO and all CO_2 products come off the surface at thermal velocities. Unfortunately, the experiments performed to date do not permit a more detailed analysis.

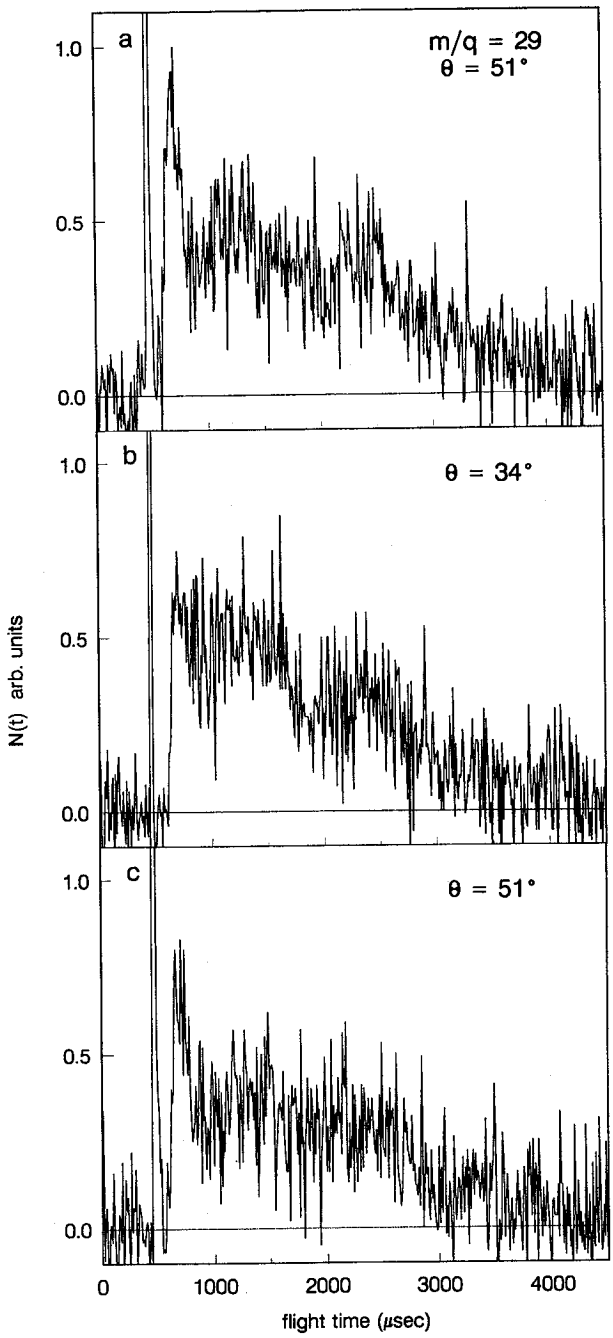

Figure 8. TOF distributions of reactively scattered ^{13}CO using BEAM III conditions. The angle of incidence of the molecular beam with the surface was 51°. The angles indicated in the figure correspond to the angle between the detector axis and the surface normal.

IV. DISCUSSION

The inelastic-scattering data imply the existence of two oxygen atom scattering channels. By analogy with previous studies,[21, 22] we interpret the fast channel as direct inelastic scattering and the slow channel as trapping desorption. The direct inelastically scattered O-atoms give up approximately 70-80 percent of their energy to the surface, while atoms that are momentarily trapped by the surface transfer essentially all their initial translational energy to the surface and desorb at roughly thermal velocities. From the fit (not shown) to the m/q=16 TOF distributions, we conclude that the direct inelastic channel accounts for 80-90 percent of the inelastic-scattering events.

Interpretation of the two peaks in the CO TOF data is less straightforward. The combination of two different reaction mechanisms provides a compelling explanation. The hyperthermal CO products may be formed through a direct reaction, in which a surface carbon atom transfers directly to an incoming O-atom and produces CO on a time scale too short to allow complete equilibration with the surface. This mechanism, known as the Eley-Rideal (ER) mechanism,[23] has only once been observed unambiguously.[24] The thermal CO may result from reaction through a more common mechanism, the Langmuir-Hinschelwood (LH) mechanism,[23] where the impinging oxygen atom is chemisorbed and then reacts to form CO, which is subsequently ejected. The time scale of this reaction would be long enough to permit complete equilibration and consequently a loss of memory of the initial O-atom energy or angle of incidence. The CO products would then desorb from the surface at thermal energies with a cosine angular distribution peaked about the surface normal. CO products formed through a direct reaction should have translational energies that are correlated with incident O-atom collision energies, and they should be scattered pref-

erentially in the specular direction. Our observations of thermal and hyperthermal CO products, along with the angular dependence of the hyperthermal peak, are consistent with the interpretation that both the ER and LH mechanisms are occurring. By narrowing the O-atom velocity distribution and increasing the energy resolution for short arrival times, we should be able to determine the dependence of CO kinetic energy on O-atom collision energy and thus make a more definitive conclusion about the reaction mechanisms.

The LH mechanism may also be operative in the production of CO_2. The TOF distribution of CO_2 exhibits only a thermal component, which probably results from the reaction of adsorbed O-atoms with CO residing on the surface. Previous work[25–27] on the oxidation of CO on a Pt(111) surface has shown that CO_2 is formed by a basically LH-associative desorption process that yields CO_2 products which are peaked about the surface normal and have energies at least four times greater than expected if the CO_2 molecule had desorbed in equilibrium with the surface.

Other possible mechanisms cannot be excluded from consideration. Energetic incident O-atoms could possibly collisionally eject CO from the surface and give rise to a fast signal that is peaked in the specular direction. Another possible explanation for the slow signal is that fast O_2 in the beam could react to produce CO (or CO_2). The products would then desorb at approximately thermal velocities. The oxidation of graphite by O_2 has been studied extensively with relatively low impact energies and high surface temperatures.[28–30]

Within the framework of the ER reaction mechanism, analysis of the energetics shows that about one third of the available energy is channeled into translational energy of the CO product. The reaction, $O(g) + C(s) \longrightarrow CO(g)$, is exothermic by 3.7 eV. Adding this energy to the average collision energy (BEAM I) of 5.9 eV yields

an available energy of 9.6 eV. The approximate CO product translational energy is 3 eV, which is about 31 percent of the available energy. The majority of the available energy must therefore be partitioned between internal excitation of the surface and of the product CO. In a study of the reaction of hyperthermal oxygen atoms with graphite, Holtzclaw, et al.[13] monitored infrared emission of CO and derived a vibrational temperature of 10,000 K ($\sim$ 0.9 eV) for the CO product. In light of the fact that we observe two channels for the production of CO, the assumption by Holtzclaw, et al. of a Boltzmann vibrational distribution is crude. Nevertheless, their data do give an indication of the level of vibrational excitation in the CO. The rotational temperature is likely to be less than or equal to the vibrational temperature; thus most of the internal energy must end up in the surface.

The assumed O + C $\longrightarrow$ CO reaction mechanisms have implications for the temperature dependence of the reactivity. The ER mechanism should be temperature independent, while the LH mechanism should depend strongly on temperature. And because collision energy could change the branching ratio between ER and LH products, the temperature dependence of the reactivity could vary with collision energy. Hence, it is not necessarily valid to draw any conclusions about the temperature dependence of the reaction from experiments performed using low collision energies.

The reaction mechanisms suggested by our data also show that the product angular distribution can be sensitive to the mechanism. If contamination from scattered products were a potential problem, then it would be useful to know whether these products would be scattered preferentially in the specular direction or towards the surface normal.

As mentioned in Section I, reactions involving scattered oxygen atoms can be a secondary source of degradation on spacecraft. Our inelastic-scattering experiments

suggest that indirect impingement may not pose a great hazard because the majority of the initial collision energy is lost on impact. The O-atoms emerging from the first surface should be less reactive with surfaces on subsequent collisions as a result of the reduced collision energy. Further work on the energy dependence of reactivity will enable us to quantify the threat of scattered O-atoms.

V. CONCLUSION

The results from our preliminary study of the reaction of hyperthermal oxygen atoms with an amorphous carbon surface can be summarized as follows. Inelastically scattered O-atoms follow two different pathways, probably direct inelastic scattering and trapping desorption. The direct inelastic component corresponds to a 70-80 percent loss of initial O-atom kinetic energy, and the trapping desorption component corresponds to O-atoms emerging from the surface with thermal velocities. The direct inelastic channel accounts for 80-90 percent of the scattering events. The dominant reactive product is CO, although some CO_2 is formed. The CO products exhibit a hyperthermal component with about 3 eV of translational energy and a slow, thermal component. The CO_2 products come off the surface with only thermal velocities. Angular data show that hyperthermal CO is scattered preferentially in the specular direction. The combination of the TOF and angular data suggests that two interaction mechanisms, an Eley-Rideal mechanism and a Langmuir-Hinschelwood mechanism, lead to the production of CO.

Clearly, future experiments would be more meaningful if the translational energy distribution of the incident O-atom beam were much narrower and if the time resolution were better. These improvements can be accomplished by using a slotted disk to chop the incident beam at various time delays from the CO_2 laser pulse and then

collecting the TOF distributions in smaller time increments. (The slotted disk will also remove any ambiguity arising from a possible synergistic relationship between O-atoms and UV and VUV light.) The ensuing high resolution data will also enable the determination of the incident O-atom energy dependence of each reaction channel, as well as the translational energy distributions of all scattered species. The energy dependence will not only clear up the assignment of the fast component seen in the CO TOF distribution, but it will allow us to answer the nagging question about whether an energy threshold exists above which the reactivity becomes energy independent. If the fast CO products are indeed formed through an ER mechanism, then the reaction probability should increase with collision energy until the O-atom energy is high enough to permit penetration of O-atoms into the surface.

The results obtained so far are crude, but they point the way to further investigations that will resolve ambiguities in the data, and they reveal the importance of understanding the interaction mechanism.

REFERENCES

1. D. R. Peplinski, G. S. Arnold, and E. N. Borson, "Satellite Exposure to Atomic Oxygen in Low Earth Orbit," in *Proceedings of the 13th Space Simulation Conference, NASA CP-2340* (Orlando, FL, 1984), pp. 133-145.

2. J. T. Visentine, "Environmental Definition of the Earth's Neutral Atmosphere" in *Proceedings of the NASA/SDIO Space Environmental Effects on Materials Workshop, NASA CP-3035* (Hampton, VA, 1988), pp. 179-195.

3. A. E. Hedin, *et al.*, "MSIS-86 Thermospheric Model," J. Geophys. Res. **92**, 4649 (1987).

4. L. J. Leger, "Oxygen Atom Reaction With Shuttle Materials at Orbital Altitudes," *NASA TM-58246*, 1982.

5. *Proceedings of the NASA Workshop on Atomic Oxygen Effects*, JPL Publication 87-14, edited by D. E. Brinza, (Pasadena, CA, 1987); *Proceedings of the NASA/SDIO Space Environmental Effects on Materials Workshop, NASA CP-3035* (Hampton, VA, 1988).

6. D. E. Hunton, "Shuttle Glow," Sci. Am., 92-98 (Nov. 1989).

7. S. Koontz, L. Leger, K. Albyn, and J. Cross, "The Role of Vacuum Ultraviolet Radiation in the Atomic Oxygen Reactivity of Candidate Space Station Materials," J. Spacecraft and Rockets **27**, 346 (1990).

8. J. B. Cross, J. A. Martin, L. E. Pope, and S. L. Koontz, "Oxidation of MoS_2 by Thermal and Hyperthermal Atomic Oxygen," in *Proceedings of the 3rd International SAMPE Electronics Conference*, 638 (1989).

9. I. Yilgor, E. Yilgor, and M. Spinu, "Synthesis and Characterization of Atomic Oxygen Resistant Poly(Siloxane-Imide) Coatings," Polymer Preprints **28**, 84 (1987).

10. J. B. Cross, E. H. Lan, C. A. Smith, and R. M. Arrowood, "Evaluation of Atomic Oxygen Interaction with Thin-Film Aluminum Oxide," in *Proceedings of the 3rd International Conference on Surface Modification Technologies* (Neuchatel, Switzerland, 1989).

11. B. A. Banks, S. K. Rutledge, and J. A. Brady, "The NASA Atomic Oxygen Effects Test Program," in *Proceedings of the 15th Space Simulation Conference, NASA CP-3015* (Williamsburg, VA, 1989), pp. 51-65.

12. O. J. Orient, A. Chutjian, and E. Murad, "Recombination reactions of 5-eV $O(^3P)$ atoms on a MgF_2 surface," Phys. Rev. A **41**, 4106 (1990).

13. K. W. Holtzclaw, M. E. Fraser, and A. Gelb, "Infrared Emission from the Reaction of High Velocity Atomic Oxygen with Graphite and Polyethylene," J. Geophys. Res. **95**, 4147 (1990).

14. E. B. D. Bourdon, R. H. Prince, W. D. Morison, and R. C. Tennyson, "Real-Time Monitor for Thin Film Etching in Atomic Oxygen Environments," Surf. and Coatings Technol. (in press).

15. A. Joshi and R. Nimmagadda, "Erosion of diamond films and graphite in oxygen plasma," J. Mater. Res. **6**, 1484 (1991).

16. L. Leger, J. Visentine, and B. Santos-Mason, "Selected Materials Issues Associated with Space Station," in *Proceedings of the 18th International SAMPE Technical Conference*, 1015 (1986).

17. D. E. Brinza, D. R. Coulter, S. Y. Chung, K. O. Smith, J. Moacanin, and R. H. Liang, "A Facility for Studies of Atomic Oxygen Interactions with Materials," in *Proceedings of the 3rd International SAMPE Electronics Conference*, 646 (1989).

18. Y. T. Lee, J. D. McDonald, P. R. LeBreton, and D. R. Herschbach, "Molecular Beam Reactive Scattering Apparatus with Electron Bombardment Detector," Rev. Sci. Instrum. **40**, 1402 (1969).

19. J. H. Sanders, P. B. Lloyd, and B. J. Tatarchuk, "Application and Performance of Silicon-Based Atomic Oxygen Protective Coatings," in *Proceedings of the 34th International SAMPE Symposium*, 1152 (1989).

20. G. E. Caledonia, R. H. Krech, and B. D. Green, "A High Flux Source of Energetic Oxygen Atoms for Material Degradation Studies," AIAA J. **25**, 59 (1987).

21. M. E. Saecker, S. T. Govoni, D. V. Kowalski, M. E. King, and G. M. Nathanson, "Molecular Beam Scattering from Liquid Surfaces," Science **252**, 1421 (1991).

22. C. T. Rettner, E. K. Schweizer, and C. B. Mullins, "Desorption and trapping of argon at a 2H-W(100) surface and a test of the applicability of detailed balance to a nonequilibrium system," J. Chem. Phys. **90**, 3800 (1989).

23. P. W. Atkins, *Physical Chemistry* (Freeman, New York, 1986) 3rd ed., pp. 782-3.

24. E. W. Kuipers, A. Vardi, A. Danon, and A. Amirav, "Surface-Molecule Proton Transfer: A Demonstration of the Eley-Rideal Mechanism," Phys. Rev. Lett. **66**, 116 (1991).

25. C. T. Campbell, G. Ertl, H. Kuipers, and J. Segner, "A molecular beam study of the catalytic oxidation of CO on a Pt(111) surface," J. Chem. Phys. **73**, 5862 (1980).

26. J. Segner, C. T. Campbell, G. Doyen, and G. Ertl, "Catalytic Oxidation of CO on Pt(111): The Influence of Surface Defects and Composition on the Reaction Dynamics," Surface Sci. **138**, 505 (1984).

27. C. A. Becker, J. P. Cowin, and L. Wharton, "CO_2 product velocity distributions for CO oxidation on platinum," J. Chem. Phys. **67**, 3394 (1977).

28. D. R. Olander, W. Siekhaus, R. H. Jones, and J. A. Schwarz, "Reactions of Modulated Molecular Beams with Pyrolytic Graphite. I. Oxidation of the Basal Plane," J. Chem. Phys. **57**, 408 (1972).

29. D. R. Olander, R. H. Jones, J. A. Schwarz, and W. J. Siekhaus, "Reactions of Modulated Molecular Beams with Pyrolytic Graphite. II. Oxidation of the Prism Plane." J. Chem. Phys. **57**, 421 (1972).

30. A. Joshi, R. Nimmagadda, and J. Herrington, "Oxidation kinetics of diamond, graphite, and chemical vapor deposited diamond films by thermal gravimetry," J. Vac. Sci. Technol. A **8**, 2137 (1990).

TECHNICAL REPORT STANDARD TITLE PAGE

1. Report No. 91-34	2. Government Accession No.	3. Recipient's Catalog No.
4. Title and Subtitle Inelastic and Reactive Scattering of Hyperthermal Oxygen From Amorphous Carbon		5. Report Date August 15, 1991 6. Performing Organization Code
7. Author(s) T. Minton, C. Nelson, D. Brinza, R. Liang		8. Performing Organization Report No.
9. Performing Organization Name and Address JET PROPULSION LABORATORY California Institute of Technology 4800 Oak Grove Drive Pasadena, California 91109		10. Work Unit No. 11. Contract or Grant No. NAS7-918 13. Type of Report and Period Covered JPL Publication
12. Sponsoring Agency Name and Address NATIONAL AERONAUTICS AND SPACE ADMINISTRATION Washington, D.C. 20546		14. Sponsoring Agency Code RE156 BK-506-43-21-03-00

15. Supplementary Notes

16. Abstract

The reaction of hyperthermal oxygen atoms with an amorphous carbon-13 surface has been studied using a modified universal crossed molecular beams apparatus. Time-of-flight distributions of inelastically scattered O-atoms and reactively scattered ^{13}CO and $^{13}CO_2$ were measured with a rotatable mass spectrometer detector. Two inelastic-scattering channels were observed, corresponding to a direct inelastic process in which the scattered O-atoms retain 20-30 percent of their initial kinetic energy and to a trapping desorption process whereby O-atoms emerge from the surface at thermal velocities. Reactive scattering data imply the formation of two kinds of CO products, 1) slow products whose translational energies are determined by the surface temperature and 2) hyperthermal (~3 eV) products with translational energies comprising roughly 30 percent of the total available energy (E_{avl}), where E_{avl} is the sum of the collision energy and the reaction exothermicity. Angular data show that the hyperthermal CO is scattered preferentially in the specular direction. CO_2 product was also observed, but at much lower intensities than CO and with only thermal velocities.

17. Key Words (Selected by Author(s))	18. Distribution Statement
Ground Support Systems and Facilities (Space) Physical Chemistry Materials (General) Atomic and Molecular Physics	Unclassified; unlimited

19. Security Classif. (of this report)	20. Security Classif. (of this page)	21. No. of Pages	22. Price
Unclassified	Unclassified	36	